ChemEurJ

Research Article
doi.org/10.1002/chem.202502078

Chemistry Europe
European Chemical Societies Publishing

www.chemeurj.org

Layer Sliding-Induced Fluorescence Changes in a Flexible Hydrogen-Bonded Organic Framework

Taito Hashimoto,[a] Mario de la Hoz Tomás,[b] Ryusei Oketani,[a] Boiko Cohen,[b] Abderrazzak Douhal,*[b] and Ichiro Hisaki*[a]

Flexible hydrogen-bonded organic frameworks (HOFs) capable of changing their fluorescence properties upon structural transformation have gained much attention, while their design strategies have not been established. Herein, we demonstrate that sliding of the robust hydrogen-bonded 2D layers can induce dynamic emission color changes of HOFs. Layered HOF **CP-tBPy-1**, which is composed of *tert*-butylpyrene derivative with four carboxyphenyl groups (**CP-tBPy**), transformed to another crystalline form, **CP-tBPy-2,** upon release of guest solvent molecules. Single-crystal X-ray diffraction analysis revealed that the sliding of the layers changed the pyrene cores from monomeric to dimeric species, giving rise to fluorescence color changes from blue to green. Fluorescence spectroscopy and single-crystals microscopy disclosed details of the photobehaviors of these HOFs. These results are the first example of fluorescence changes of HOFs due to sliding of hydrogen-bonded 2D network layers, providing a new design strategy to construct functional fluorescent porous materials.

1. Introduction

Flexible porous frameworks have attracted attention because they can show interesting dynamic physicochemical properties involving stimuli-induced pore breathing and reversible phase transformation.[1–3] Such frameworks have been actively studied on metal-organic frameworks (MOFs)[4–6] and covalent-organic frameworks (COFs).[7–9] So far, selective and efficient gas sorption,[10] control of material deliveries,[11] and sensing[12] have been achieved by flexible framework materials.

Hydrogen-bonded organic frameworks (HOFs)[13–19] constructed through reversible hydrogen-bond (H-bond) are a new type of flexible porous frameworks.[20–22] HOFs can present dynamic and unique structural transformations due to reversible H-bonds.[23–25] In many cases, HOFs undergo structural transformation by release of the guest solvent molecules accommodated within their pores, i.e., desolvation. Chen and coworkers reported that HOF-5 showed significant framework contraction by the desolvation, and that the activated HOF encapsulated a high density of carbon dioxide molecules.[26] 2D layered HOFs composed of tetracarboxylic acids with *o*-bis(4-carboxyphenyl)aryl groups were recently reported to show drastic structural transformation with H-bond rearrangement upon desolvation.[25,27–29]

Some flexible HOFs can change their fluorescence properties, making them a candidate for sensor materials.[30] The fluorescence changes are caused by conformational change in the fluorophore structure, such as rotation of the aryl group in a tetraphenylethene (TPE) (Figure 1a), and by rearrangements of weakly hydrogen-bonded frameworks (Figure 1b).[31–40] Z. Chi and coworkers reported on **8PN** HOFs, composed of tetrakis(nitrobiphenyl)-substituted TPE, and showed versatile reversible transformations accompanied by a change in their luminescence properties with the guest molecule.[31] P. Xue and coworkers have reported that a HOF based on a phenothiazine derivative with three cyano groups displays fluorescence color changes from blue to green upon exposure to benzene vapor.[38] However, dynamic fluorescence changes have not been achieved in HOFs that possess the well-defined, robust, H-bonded network structures, despite the ease of design due to their robustness. Exploring such systems is paramount to establishing design strategies of fluorescence-tunable flexible HOFs.

Pyrene and its derivatives have been used in a wide range of science and technology, including applications in biology,[41,42] detection of chemical compounds,[43] optical materials,[44,45] and porous materials.[43,46–49] The well-known, distinguishable monomer and excimer emissions make pyrene derivatives attractive for suitable building blocks of new HOFs showing tunable fluorescence color due to small changes in the conformation of their molecular H-bonded units. Recently, we constructed a layered HOF using 4,5,9,10-tetrakis(4- carboxyphenyl)pyrene and showed the contraction of its framework (**CP-Py-1**) upon

[a] T. Hashimoto, Dr. R. Oketani, Prof. Dr. I. Hisaki
Division of Chemistry, Graduate School of Engineering Science, The University of Osaka, 1–3 Machikaneyama, Toyonaka, Osaka 560–8531, Japan
E-mail: i.hisaki.es@osaka-u.ac.jp

[b] M. de la Hoz Tomás, Prof. Dr. B. Cohen, Prof. Dr. A. Douhal
Departamento de Química Física, Facultad de Ciencias Ambientales y Bioquímica, and INAMOL, Universidad de Castilla-La Mancha, Avenida Carlos III, Toledo 45071, Spain
E-mail: abderrazzak.douhal@uclm.es

Taito Hashimoto and Mario de la Hoz Tomás contributed equally to this work.

Supporting information for this article is available on the WWW under https://doi.org/10.1002/chem.202502078

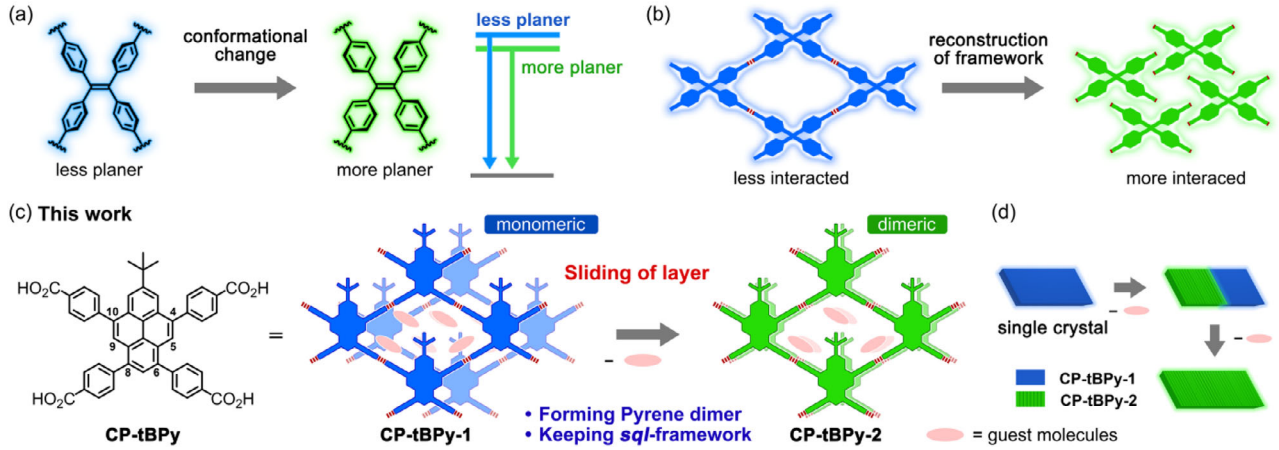

Figure 1. a, b) Conventional mechanism of fluorescence color changes of HOFs based on a) conformational changes in the fluorophore structure and b) rearrangements of molecular assembly connected through weak interactions. c) Transformation of *tert*-butylpyrene-based **CP-tBPy-1** into another **CP-tBPy-2** by spontaneous desolvation. Sliding of the well-defined layers changed the pyrene cores from monomeric to dimeric, allowing fluorescence color changes from blue to green. d) Illustration of a single crystal of the **CP-tBPy-1** undergoing sliding motion of the layers producing fluorescence color changes.

desolvation, while no change in its monomeric fluorescence color was observed as the molecular stacking was retained in the transformations due to the sterically crowded arms.[48]

Here, applying a small change in the above strategy, we designed a new 2D layered HOF based on 4,6,8,10-tetrakis(4-carboxyphenyl)-2-*tert*-butylpyrene (**CP-tBPy**) (Figure 1c). Introducing the bulky *tert*-butyl group at the 2-position of the pyrene core and four carboxyphenyl groups at spatially distant 4,6,8,10-positions should increase the freedom of molecular arrangement, making it possible to modulate the relative position of the stacked pyrene cores. Indeed, we found that the desolvation-induced structural transformation of HOF **CP-tBPy-1** into **CP-tBPy-2** brought fluorescence color changes from blue to green by sliding motion of the H-bonded layers. The transformation can be monitored by gradual fluorescence change on a single crystal (Figure 1d). Time-resolved spectroscopy and single-crystal fluorescence microscopy reveal excimer formation along with emission from monomers and preformed dimers in the HOFs. The associated times become shorter as the HOF is activated by the desolvation of **CP-tBPy-1** producing **CP-tBPy-2**. This work is the first example of HOFs showing fluorescence color changes due to 2D layer sliding, providing a new strategy and knowledge to construct functional fluorescent flexible frameworks of potential applications in lighting or sensing.

2. Results and Discussion

2.1. Crystallography of CP-tBPy-1 and CP-tBPy-2

CP-tBPy was synthesized according to the literature (Scheme S1),[50,51] and recrystallized at 60 °C using a mixed solution of *N*,*N*-dimethylformamide (DMF) and methyl benzoate (MeBz) to give single crystals of HOF **CP-tBPy-1** suitable for single-crystal X-ray diffraction (SCXRD) analysis (Table S1). Figures 2a and S1 show the crystal structure of **CP-tBPy-1**. The framework is composed of crystallographically independent two molecules of **CP-tBPy** (Figure S1a). Carboxy groups of **CP-tBPy** form self-complementary H-bonded dimer with O···O distances of 2.56 Å to 2.67 Å to give a 2D sheet structure with an ***sql***-topological network. The sheet possesses rhombic apertures with a size of 21.7 Å and 34.2 Å (Figure S1b). In the HOF, 2D sheets are slipped–stacked with few overlap of the pyrene moieties in the adjacent layers (Figures 1b and S1c). The first and second layers are stacked in the manner that **CP-tBPy** molecules are aligned in the same direction (Figure S1c). Third-fourth layers and first-second layers are related by the inversion symmetry operation. **CP-tBPy-1** possesses 1D inclusion channels along the *a* axis with 53% void ratio (Figure S1d). The molecules of MeBz are accommodated in the channel with a host / guest molar ratio of 2 / 8.5 (Figure S1a).

After picking out from the crystallization solvent, the single crystals of **CP-tBPy-1** transform to **CP-tBPy-2** under ambient conditions (Figure 2g), accompanied by the formation of cracks. The cracks are nearly parallel to the (1 0 -1) plane that corresponds to the H-bonded 2D layers (Figure S3). The crystal's color also changed from colorless (**CP-tBPy-1**) to yellow (**CP-tBPy-2**) (Figure S4). The resultant platelet pieces retained single-crystallinity, allowing SCXRD analysis of **CP-tBPy-2** (Figures 2d and S2). **CP-tBPy-2** is composed of the one independent molecule of **CP-tBPy** (Figure S2a). The ***sql***-topological 2D network structure is nearly the same as that of **CP-tBPy-1** (Figures S1b, S2b). On the other hand, the stacking manner of the sheets in **CP-tBPy-2** is different from that in **CP-tBPy-1** (Figures S1c, S2c). The distance between the first and second layers along the longer diagonal direction becomes shorter and changes from 5.1 Å to 2.0 Å, resulting in the overlapping of the pyrene cores (Figures 2b, 2e). The center-to-center distance between the pyrene cores decreased from 6.8 Å to 4.2 Å (Figures 2c, f). In the second and third layers, the distance along the longer diagonal direction decreases from 4.8 Å to 1.9 Å, and that along the shorter diagonal direction increases from 1.1 Å to 5.9 Å (Figures 2b, 2e). The distance between the pyrene cores slightly decreases from 7.1 Å to 6.8 Å (Figures 2c, 2f). The layer sliding may be supported by rotation of peripheral phenylene rings: dihedral angles between the peripheral phenylene ring and the core in **CP-tBPy-1**

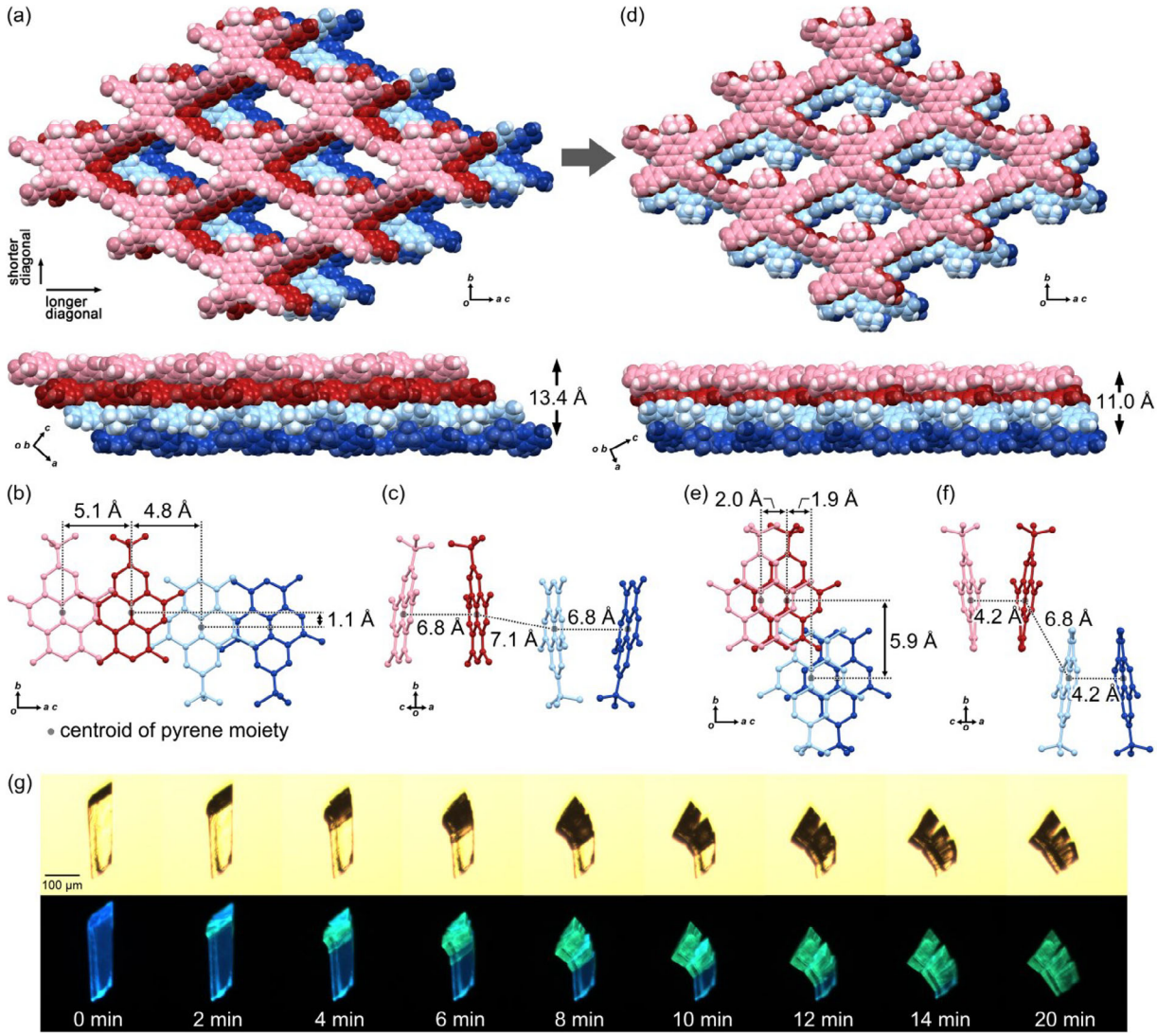

Figure 2. a-e) Crystal structures of HOFs **CP-tBPy-1** and **CP-tBPy-2 HOFs**. a) Packing diagrams of **CP-tBPy-1**. b, c) The stacking manners of **CP-tBPy** molecules in **CP-tBPy-1**. d) Packing diagrams of **CP-tBPy-2**. e, f) The stacking manners of **CP-tBPy** molecules in **CP-tBPy-2**. g) Time course of morphological and fluorescence changes of a single crystal of **CP-tBPy-1** upon spontaneous release of the guest molecules under ambient light (top) and UV light (bottom). The peripheral carboxyphenyl groups are omitted in b), c), e), and f).

(45–59°) became slightly smaller in **CP-tBPy-2** (42–47°) (Figure S5). **CP-tBPy-2** has 1D channels along the *a* axis with 38% void ratio (Figure S2d). The molecules of MeBz accommodated in the channel were not crystallographically solved due to the severe disorder. The host / guest molar ratio of **CP-tBPy-2** / MeBz can be estimated to be 1 / 3, assuming that MeBz molecules are accommodated in the void with a packing coefficient of 70%.[52] To investigate a possibility of reversible transformation between **CP-tBPy-1** and **CP-tBPy-2**, bulk crystals of the latter were soaked in MeBz solvent for 6 hours. The soaked sample showed almost the same PXRD pattern as **CP-tBPy-2** (Figure S8a), indicating that this transformation is irreversible.

2.2. Thermal Stability

The bulk crystalline sample of **CP-tBPy-1** was subject to thermal gravimetric (TG) analysis. The TG curve reaches a plateau at ca. 230 °C with weight loss of 47 % (Figure 3a), indicating that **CP-tBPy-1** HOF contains MeBz molecules with a host / guest molar ratio of 1 / 4.28. This ratio is consistent with that determined by SCXRD analysis (Figure S1a). Variable-temperature powder X-ray diffraction (VT-PXRD) measurement showed the two-step structural changes from the initial structure (**CP-tBPy-1**) to the second one (**CP-tBPy-2**) at around 80 °C, and then to the third one (**CP-tBPy-3**) at around 240 °C (Figure 3b). Representative PXRD patterns of the observed structures are shown in Figure 3c, where the patterns of initial and second phases are consistent with the simulated ones calculated from SCXRD data of **CP-tBPy-1** and **CP-tBPy-2**, respectively (Figure S7). **CP-tBPy-3** retained its structure around 400 °C, although the crystal structure could not be determined due to its low single-crystallinity. **CP-tBPy-3** soaked in MeBz solvent did not change back to **CP-tBPy-2** and showed the same PXRD pattern as **CP-tBPy-3** (Figure S8b), indicating that the transformation of **CP-tBPy-2** to **CP-tBPy-3** is also irreversible.

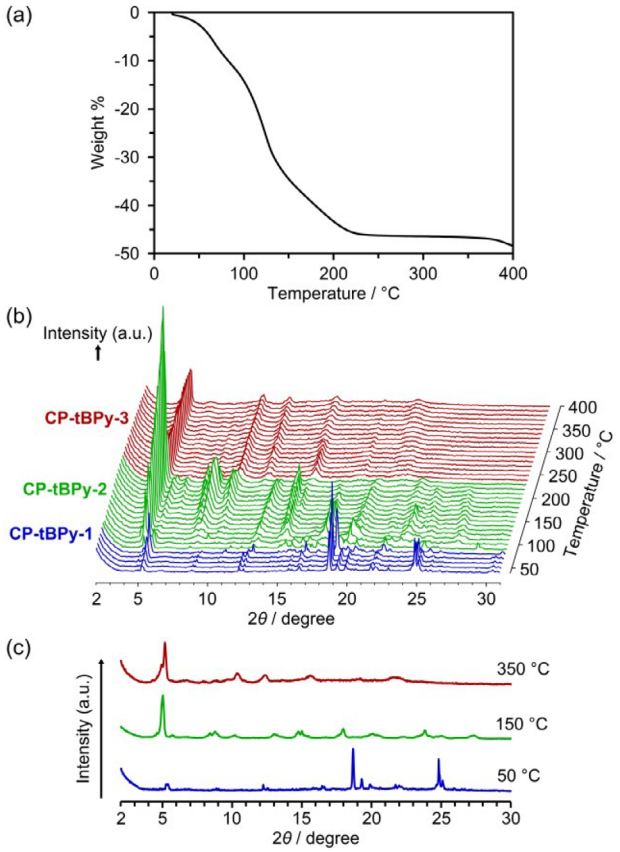

Figure 3. a) TG curve of **CP-tBPy-1**. b) VT-PXRD measurement of **CP-tBPy-1**. c) Representative PXRD patterns of **CP-tBPy-1**, **CP-tBPy-2** and **CP-tBPy-3** observed in VT-PXRD measurement.

CP-tBPy-2 bulk crystal was activated at 130 °C under vacuum conditions to give the activated HOF **CP-tBPy-2a**. Complete removal of the solvent molecules was confirmed by ^{1}H NMR experiments (Figure S23). PXRD measurement indicates that **CP-tBPy-2a** retained its original structure (Figure S9). Heating **CP-tBPy-2a** at 260 °C for 2 hours gives **CP-tBPy-3** (Figure S9). These results show that the initial transformation from **CP-tBPy-1** to **CP-tBPy-2** is triggered by a release of the guest molecules while the second one from **CP-tBPy-2** to **CP-tBPy-3** is heat-related.

2.3. Stacking Interaction Energy

Stacked dimers of **CP-tBPy** molecules have different types of intermolecular interactions in HOFs **CP-tBPy-1** and **CP-tBPy-2**. The former has CH···O, CH···C, and CH···π interactions, while the latter has C···C and CH···π interactions (Figure S6). This difference is brought by the sliding of the 2D layers and the conformational changes of peripheral phenylene rings.

To investigate the structural stability of the framework before and after the transformation, we calculated the interaction energies of stacked dimers in **CP-tBPy-1** and **CP-tBPy-2**.[53,54] Note that these HOFs have two types of stacking, one composed of two **CP-tBPy** directing parallel (named as **CP-tBPy-1**_para and **CP-tBPy-2**_para) and the other antiparallel (named as **CP-tBPy-1**_anti and **CP-tBPy-2**_anti). The structural details of the stacked dimer models are provided in Figure S10.

Table 1. Interaction energies (kcal mol^{-1}) for the stacked two molecules in anti or parallel arrangements.

Dimer model	E_{dimer}
CP-tBPy-1_para	−32.92
CP-tBPy-1_anti	−31.18
CP-tBPy-2_para	−42.65
CP-tBPy-2_anti	−34.12

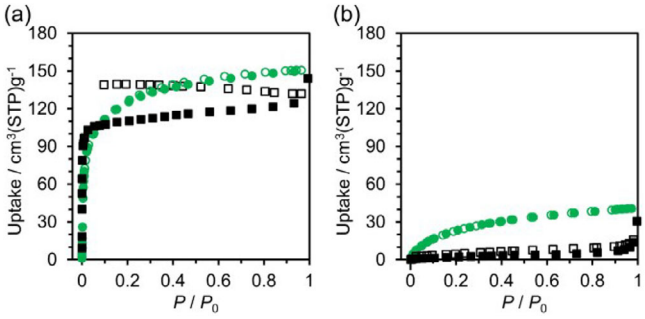

Figure 4. Gas sorption isotherms of the activated HOFs for nitrogen (black) at 77 K and carbon dioxide (green) at 195 K. a) **CP-tBPy-2a** and b) **CP-tBPy-3**. Solid and open symbols correspond to adsorption and desorption processes, respectively.

The E_{dimer} value for each of the dimer models is calculated at the B97D/6–311 + G(d,p) level of theory (Table 1). In both parallel and antiparallel stacking dimer models, **CP-tBPy-2** has larger E_{dimer} values than **CP-tBPy-1**. In particular, **CP-tBPy-2**_para has a larger E_{dimer} value than **CP-tBPy-1**_para by 9.73 kcalmol^{-1}. These results indicate that due to the strong interactions of the stacked dimers, the structural transformation is irreversible (Figure S8a) and enables **CP-tBPy-2** to remain in its original structure after activation of the void (Figure S9).

2.4. Porosity

CP-tBPy-2a and **CP-tBPy-3** were subject to N_2 and CO_2 sorption experiments at 77 K and 195 K, respectively (Figure 4). The isotherms of **CP-tBPy-2a** show a rapid rise at low pressures and can be categorized as a type-I isotherm and reached to the uptake of 144 cm^{3}g^{-1} and 154 cm^{3}g^{-1} at P/P_0 = 1.0, respectively (Figure 4a). **CP-tBPy-3** showed no adsorption of N_2, while it showed a small adsorption of CO_2 and the uptakes reached 44 cm^{3}g^{-1} at P/P_0 = 1.0 (Figure 4b). The low adsorption ability of **CP-tBPy-3** is likely due to its small void space and low crystallinity.

Its Brunauer-Emmett-Teller (BET) surface area was calculated to be 433 m^{2}g^{-1} and 605 m^{2}g^{-1} based on the N_2 and CO_2 sorption experiments, respectively, for **CP-tBPy-2a** (Figure S11).

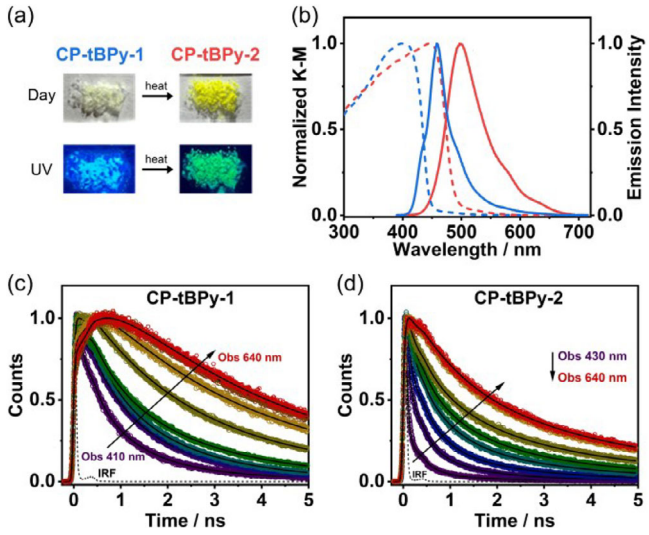

Figure 5. a) Fluorescence photographs of bulk crystals of **CP-tBPy-1** and **CP-tBPy-2** at naked eye and under UV light. b) Normalized diffuse reflectance (converted to K–M function, dashed line) and emission (solid line) spectra of **CP-tBPy-1** (blue) and **CP-tBPy-2** (red) in solid state. For the emission spectra, the excitation wavelength was 370 nm. Magic-angle ps-emission decays of c) **CP-tBPy-1** and d) **Cp-tBPy-2** in solid state, upon excitation at 371 nm and observation at 410, 430, 460, 490, 520, 550, 580, 610, and 640 nm. The solid lines are from the best multiexponential fits, and IRF is the instrumental response function (~ 70 ps).

2.5. Photophysical Properties in Solid State

Next, we investigated the fluorescence change due to the **CP-tBPy-1** to **CP-tBPy-2** transformation. Interestingly, as the crystals crack, the blue fluorescence changes to green due to the structural transformation as shown in snapshots of single crystal under UV light (Figure 2g). To explore the photophysical behavior of the HOFs and study how molecular rearrangements in the transformation affect their luminescent properties, we carried out steady-state and time-resolved emission experiments on HOFs **CP-tBPy-1** and **CP-tBPy-2** in solid state (Figure 5).

The diffuse reflectance spectra show a broad band with maximum intensities at 398 and 445 nm for **CP-tBPy-1** and **CP-tBPy-2**, respectively (Figure 5b and Table S2). We explain the observed red shift in the spectrum of **CP-tBPy-2** when compared to that of **CP-tBPy-1** in terms of a shorter distance between the layers and a stronger overlap between the interlayer pyrene cores in the former that lead to the formation of stronger pyrene dimers. These results agree with theoretical calculations that predict a red shift in the absorption spectra of the dimers when compared to pyrene monomers.[55] **CP-tBPy-1** exhibits an intense blue emission band with a maximum intensity at 458 nm, and a long tail in the range of 550–600 nm. The main blue-emission band, having a partially preserved vibrational structure, originates from excited pyrene monomers, while the weak emission tail at longer wavelengths is likely due to excimer (M*M) species as a result of the interaction between excited (M*) and not excited (M) monomers and dimers already formed at the ground state. Similar blue-emission profiles are observed from **CP-tBPy** in diluted DMF solutions where the emissions come from M* (Figure S12 and Table S2). The presence of different types of excimers has been previously reported in pyrene-based polymers and silica film, and explained in terms of different spatial overlaps between the pyrene cores ("ideal" and "nonideal" π-π stacking).[56–58] **CP-tBPy-2** exhibits a green and broader emission band with a maximum at 500 nm, associated with the emission of dimer/excimer species (Figure 5b). Note that the emission from the monomers is absent or very weak, which indicates that the coupling between the pyrene monomers is stronger than in **CP-tBPy-1** and therefore the formation of excimers (M*M) should be significantly faster. Comparable behavior has been observed in the amorphous solid state of **CP-tBPy** (Figure S13 and Table S2). As previously discussed, this is mainly due to the existence of preformed dimers in the ground state and is in agreement with reports on other pyrene materials.[58,59]

To further characterize the photophysical properties of **CP-tBPy-1** and **CP-tBPy-2** in solid state, we performed picosecond (ps) time-resolved emission experiments (Figures 5c, d and Figure S14). The multiexponential photodynamic behavior of both HOFs depends on the observed region. For **CP-tBPy-1** from 410 to 550 nm (region I, mainly monomer emission), we got three decaying components with time constants of 0.54, 1.51, and 3.25 while from 580 to 640 nm (region II, emission from excimers), we obtained 0.4–0.6 ns for a rising component, and two decay times of 3.25 and 7.43 ns (Table 2).

The sub-nanosecond (0.4–0.6 ns) decaying and rising component reflects the presence of a common channel, which we assign to the formation of excimers (M*M). The 1.51 ns component recorded only in region I, reflects the emission lifetime of the monomers that give rise to excimer formation. We observed similar values for the monomers of **CP-tBPy** in DMF solutions (Figure S12 and Table S3). Based on the relative contribution of the 3.25 ns component, which is higher in region II, it most probably corresponds to the lifetime of preformed dimer species. Finally, the 7.43 ns component, only observed in region II, is attributed to the excimer's emission lifetime formed in 0.4–0.6 ns. The **CP-tBPy** monomers in amorphous solid state present similar photobehavior, indicating that their photodynamics is also dominated by excimer formation processes (Figure S15 and Table S4). Now, we discuss the emission decays of **CP-tBPy-2** (Table 2). The analysis of the decays in region I gives time constants of 0.05, 0.51, 2.46 ns. The picosecond component (0.05 ns) is most probably due to a fast excimer formation in strongly coupled dimers at the ground state. The 0.51 ns component reflects the emission lifetime of the monomer species to produce excimers. In similarity with the photodynamics of **CP-tBPy-1**, we assign the 2.46 ns component, with higher relative amplitude in region II, to the lifetime of preformed dimer species. The contribution of these dimers is significantly higher for **CP-tBPy-2** due to the shorter distances between the pyrene cores in the crystal structure (Table 2). This is further supported by the red shift observed in the absorption spectra (Figure 5b). In region II (520–640 nm), the 50-ps component is not present, while we observe a new decaying component of 7.2 ns, assigned to the lifetime of excimer species. Notice that for **CP-tBPy-2** in region II, the analysis did not give a short rising component, which may correspond to the 50 ps decay in region I, most probably because of a mathematical cancelation due to the overlap with the

Table 2. Values of time constants (τ_i), normalized (to 100) preexponential factors (a_i) and fractional contributions (c_i) obtained from the best fits of the emission decays of **CP-tBPy-1** and **CP-tBPy-2** in solid state upon excitation at 371 nm, and observation as indicated.

Sample	λ_{obs} / nm	τ_1 / ns	a_1	c_1	τ_2 / ns	a_2	c_2	τ_3 / ns	a_3	c_3	τ_4 / ns	a_4	c_4
	410		50	25		47	66		3	9		–	
	430		37	15		54	62		9	23		–	
	460	0.54	31	12		56	59		13	29		–	
	490		22	8		62	59		16	33		–	
CP-tBPy-1	520		20	6	1.51	59	53	3.25	21	41	7.43	–	
	550		–			50	27		40	46		10	27
	580	0.37	–100	–100		–			82	67		18	33
	610	0.47	–100	–100		–			80	64		20	36
	640	0.59	–100	–100		–			74	55		26	45
	430		87	29		11	38		2	33		-	
	460	0.05	65	10		29	45		6	45		-	
	490		42	4		44	38		14	58		-	
CP-tBPy-2	520		-		0.51	72	31	2.46	25	53	7.20	3	16
	550		-			62	21		33	55		5	24
	580		-			48	12		41	50		11	38
	610		-			24	4		59	51		17	45
	640		-			21	3		59	48		20	49

decaying components of the monomers in this spectral region. Based on the steady-state and time-resolved emission data, we draw the following picture. Monomer species, which emit in the blue region (region I), show lifetimes of 1.51 and 0.51 ns (for **CP-tBPy-1** and **CP-tBPy-2**, respectively) and are susceptible to excimer formation. In agreement with the structures of the HOFs network derived from SCXRD studies, in the not activated HOF, **CP-tBPy-1,** excimer formation occurs in about 500 ps. In the activated one, **CP-tBPy-2,** where the interlayer distance between the pyrene cores is shorter with better overlap (Figures 2b, c, e, f), this process is ten times faster and takes place in about 50 ps. These results agree with previous reports demonstrating that the molecular distance and orientation between the monomers play a key role in the pyrene excimer formation process.[60–63] Both the slow and the fast channels produce excimer species of similar emission lifetimes (~ 7 ns). We also observed preformed dimers at ground state emitting with lifetimes of 3.3 and 2.5 ns for **CP-tBPy-1** and **CP-tBPy-2**, respectively (Scheme 1).

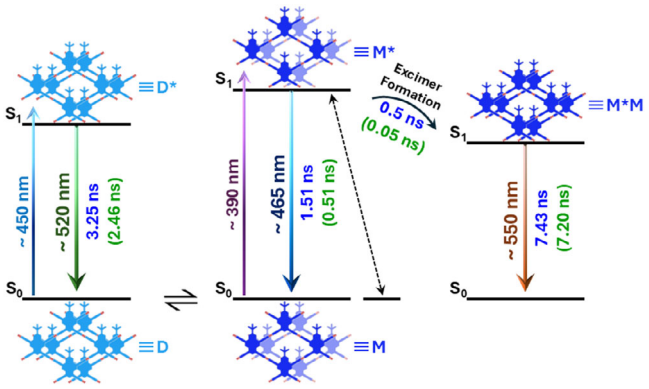

Scheme 1. Illustration (not in scale) of the involved photodynamics between the ground (S_0) and electronically first excited (S_1) states of **CP-tBPy** HOF in solid state, and in which M, D, and M*M correspond to monomer, dimer and excimer species. The lifetime values in blue and green colors correspond to those in **CP-tBPy-1** and **CP-tBPy-2**, respectively. The emission wavelength values of the intensity maxima of the bands were estimated based on the contributions of the related lifetime components in the emission decays.

2.6. Fluorescence of Single Crystals

We carried out picosecond time-resolved fluorescence microscopy experiments on single crystals of both HOFs. Figure 6 shows the images, emission spectra, and decays of a representative single crystal of **CP-tBPy-1** recorded at different times of observation.

The emission color of the **CP-tBPy-1** at ambient conditions changes with time from blue to green, suggesting a release of guest solvent molecules, producing **CP-tBPy-2** (Figure 6a). To obtain more information about the relevance of the structural transformation process on the photobehavior of the HOF, we recorded the emission spectra of **CP-tBPy-1** single crystal as a function of the observation time (Figure 6b). Initially, the single crystal shows an intense blue emission with a maximum intensity at 465 nm and a weak emission signal between 500 and 650 nm. The 465-nm band is attributed to the emission from the excited pyrene monomers, while the green one originates from pyrene excimers. The emission spectra recorded at longer observation times show a change in the color accompanied by a decrease in the 465-nm band intensity (monomers). The emission color gradually changes to green, and after 5 hours the green spectrum of the excimers becomes predominant (Figure 6b). Note that the excimer species are less emissive than

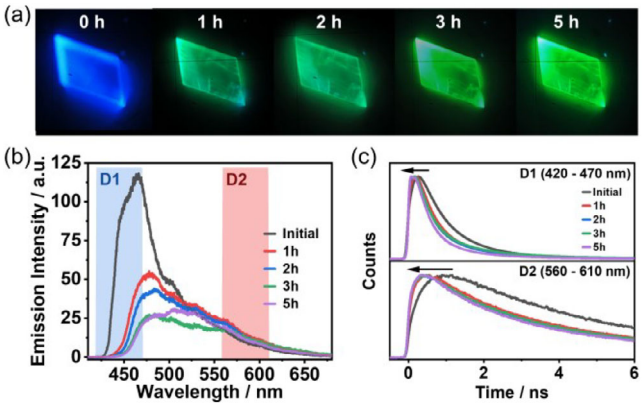

Figure 6. a) Time-dependent fluorescence photographs, b) emission spectra, and c) fluorescence emission decays of **CP-tBPy-1** single crystal. Emission decays were collected using two different filters (D1: 420–470 nm and D2: 560–610 nm). The excitation wavelength was 390 nm.

Table 3. Values of time constants (τ_i) and normalized (to 100) preexponential factors (a_i) obtained from the fit of the emission decays at different times of the **CP-tBPy-1** single-crystal shown in Figure 6.

	Region 1 (420-470 nm)				Region 2 (560-610 nm)			
Sample	τ_1 / ns	a_1	τ_2 / ns	a_2	τ_3 / ns	a_3	τ_1 / ns	a_1	τ_2 / ns	a_2	τ_3 / ns	a_3
Initial	0.6	66	1.3	33	3.1	1	0.5	−100	3.1	82	8.8	18
1h	0.5	81		17		2	-			78		22
2h	0.4	73		24		3	-			80		20
3h	0.4	63		31		6	-			81		19
5h	0.3	79		18		3	-			81		19

the monomer ones, as reflected in the fluorescence quantum yields of **CP-tBPy-2** (24%) and of **CP-tBPy-1** (45%, Table S2).

We also collected the emission decays of **CP-tBPy-1** single crystals at different times using two different filters to selectively monitor the emission of the monomers in the region of 420–470 nm (D1, region 1), and of the excimers between 560–610 nm (D2, region 2) (Figure 6c). For a fresh crystal, the decays collected in region 1 are shorter, indicating that the emission mainly comes from the monomers, whereas those in region 2 are longer and arise from the excimers (Table 3). In agreement with the behavior of the emission spectra, upon leaving the crystal at ambient conditions, the decays profile in both regions changes with time. For a fresh sample, we obtained three-time constants in region 1: ~ 0.6, ~ 1 and ~ 3 ns, all of them as decays. However, in region 2, we got time constants of ~ 0.5 (rise), ~ 3, and ~ 9 ns (decays). We assign the fastest component, present as a decay in region 1 and as a rise in region 2, to the excimer formation process, the 1-ns component to the lifetime of the pyrene monomer, and the longer ones (~3 and ~9 ns) to the lifetime of the preformed dimers and excimers species, respectively. Note that the component reflecting the excimer formation becomes shorter with the observation time (0.6 ns at 0 hours and 0.3 ns at 5 hours, region 1), indicating that the distance between the pyrene cores decreases following the release of the guest solvent molecules resulting in a stronger coupling between the

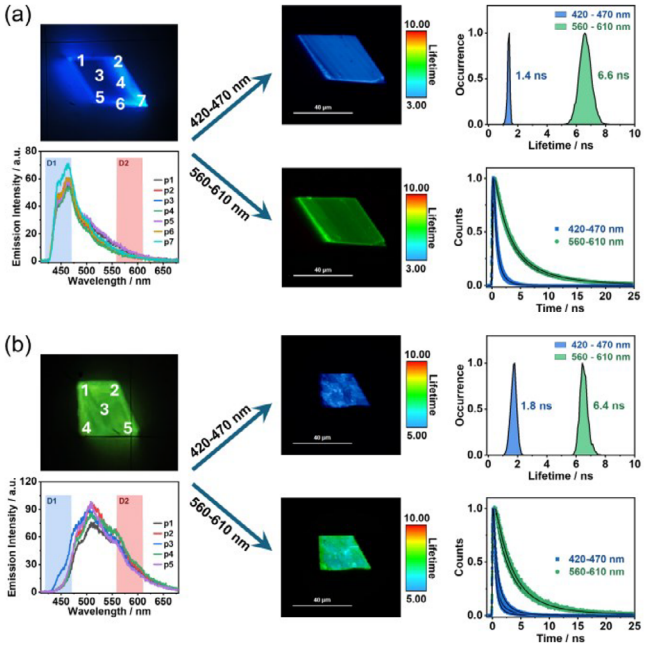

Figure 7. Fluorescence lifetime imaging microscopy (FLIM), emission spectra and fluorescence emission decays of a) **CP-tBPy-1** and b) **CP-tBPy-2** recorded at different points of the crystals. Emission decays were collected using two different filters (D1: 420–470 nm and D2: 560–610 nm). The solid lines are from the best fit using a multiexponential function. The excitation wavelength was 390 nm. The scale bar in the FLIM images is 40 µm.

pyrene cores, and therefore faster excimer formation. Similar behavior has been observed for naphthalene-based HOFs, which also show excimers formation at single-crystal level.[64] Inter-crystal excimers formation in pyrene-derivative-based HOF has been previously reported.[47] However, our results represent the first example of excimer formation at the single-crystal level in pyrene-based HOFs.

Next, we performed fluorescence microscopy experiments at different sites of **CP-tBPy-1** and **CP-tBPy-2** single crystals (Figure 7). The fluorescence lifetime imaging microscopy (FLIM) image of **CP-tBPy-1** shows a homogeneous lifetime distribution over the entire crystal surface (Figure 7a). The analysis of the average lifetime distribution produces two histograms centered on 1.4 ns in region 1 (monomer species) and 6.6 ns in region 2 (excimer species). The emission spectra collected at different points within the same crystal do not show a significant dependence on the point of photon collection, indicating that the emission has the same origin.

Similarly, **CP-tBPy-2** single crystal does not exhibit significant changes between the different interrogated positions within the space- (300 nm) and time- (IRF ~ 300 ps) resolutions of the setup (Figure 7b). The FLIM analysis shows a homogeneous average lifetime distribution centered on 1.8 ns in region 1 and 6.8 ns in region 2, similar to those obtained for **CP-tBPy-1**. The spectral behavior, on the other hand, is different from that observed for **CP-tBPy-1**. The maximum emission intensity is now located at 500 nm with shoulders at 450 and 550 nm, indicating stronger contribution from the excimer populations. The homogeneous distribution of the emitting species is confirmed by the lack of dependence on the spectral behavior at different observation

Table 4. Values of time constants (τ_i) and normalized (to 100) preexponential factors (a_i) obtained from the fits of the emission decays at different points of the **CP-tBPy-1** and **CP-tBPy-2** single-crystals shown in Figure 7.

	Region 1 (420-470 nm)						Region 2 (560-610 nm)					
Sample	t_1 / ns	a_1	t_2 / ns	a_2	t_3 / ns	a_3	t_1 / ns	a_1	t_2 / ns	a_2	t_3 / ns	a_3
CP-tBPy-1	0.5	68-80	1.2	19-30	3.4	1-2	1.2	21-38	3.0	45-65	8.8	12-20
CP-tBPy-2	0.3	62-85	1.4	14-35	3.2	1-3	-		3.3	78-82	9.3	18-22

points within the same crystal. In the obtained time constants of **CP-tBPy-1** and **CP-tBPy-2**, 0.5 ns and 0.3 ns are ascribed to excimer formation, 1.2 ns and 1.4 ns to monomers lifetime, 3.2 ns and 3.3 ns to preformed dimers lifetime and 8.8 ns and 9.3 ns to excimers lifetime for **CP-tBPy-1** and **CP-tBPy-2,** respectively (Table 4 and Table S5), as discussed in the studies of entire single crystal in Figure 6. The 0.3 ns component of **CP-tBPy2**, ascribed to excimers formation, is slightly shorter than that of **CP-tBPy-1** (0.5 ns), reflecting a shortening of the distance between the pyrene cores in the **CP-tBPy-2** single crystal. The 1.4 ns component, only observed in region 1 in **CP-tBPy-2**, corresponds to the lifetime of small population of monomers that emit at 450 nm and is absent in region 2 (Figure 7b). These results are consistent with those obtained from entire single crystal-studies and support the homogeneity of the emitting species on a single crystal. Figures S16, S17 and Tables S6, S7 show more examples of the photobehavior for several **CP-tBPy-1** and **CP-tBPy-2** single crystals. Photobehavior of other **CP-tBPy-1** and **CP-tBPy-2** single crystals was also investigated (Figures S16,17 and Tables S6, S7).

Finally, to get information on the local orientation of the pyrene cores within a single crystal, we performed emission anisotropy experiments on **CP-tBPy-1** and **CP-tBPy-2** (Figure S18). All the crystals show anisotropic emission behaviors, which also depend on the crystal orientation. The strongest dependence on the crystal orientation is observed for **CP-tBPy-1** showing distributions centered on − 0.1 (vertical orientation) and 0.6 (horizontal orientation) and indicating an ordered crystalline structure. On the other hand, the anisotropy value distributions of **CP-tBPy-2** are broad and range from 0.2 to 0.8 with only a slight dependence on the crystal orientation, indicating lower crystallinity due to the structural transformations. Similar anisotropic behavior has been described for other HOF materials.[64–66]

3. Conclusion

In this contribution, we report on dynamic fluorescence changes of a HOF upon structural transformation caused by sliding motion of the well-defined robust H-bonded network layers. HOF **CP-tBPy-1**, composed of tetratopic carboxylic acid **CP-tBPy,** transforms into **CP-tBPy-2** upon release of the guest solvent, and fully activated **CP-tBPy-2a** changes into **CP-tBPy-3** by heating. SCXRD analysis revealed that the **CP-tBPy-1** to **CP-tBPy-2** transformation is due to sliding of H-bonded 2D layers and strongly coupled pyrene dimers are formed in the latter. As a result, the fluorescence color changes from blue (**CP-tBPy-1**) to green (**CP-tBPy-2**). Time-resolved emission spectroscopy and single-crystals fluirescence microscopy studies revealed the presence of different emitting species in both HOFs. The unique configuration of the pyrene cores in **CP-tBPy-1** allows for excimer formation in ~0.5 ns. In **CP-tBPy-2** this process becomes 10 times faster due to reduced distances between the pyrene cores. The stronger coupling in the activated HOF is reflected in the shorter emission lifetimes of the emitting species, except for the excimer lifetime that remains unchanged. These results demonstrate that the flexibility of 2D layered structure is a key factor in producing dynamic fluorescent change in HOFs, providing important insight to design functional flexible porous material.

Supporting Information

Deposition numbers 2 450 567 (for **CP-tBPy-1**), and 2 450 568 (for **CP-tBPy-2**) contain the supplementary crystallographic data for this paper. These data are provided free of charge by the joint Cambridge Crystallographic Data Centre and Fachinformationszentrum Karlsruhe Access Structures service. The authors have cited additional references within the Supporting Information.[67–77]

Acknowledgments

This work was supported by KAKENHI (JP23H04029, JP24K01468, JP25H01672, and JP25H02042) from JSPS and MEXT Japan, and by grant PID2020-116519RB-I00 funded by MICIU/AEI/10.13039/501100011033 and the European Union (EU), SBPLY/23/180225/000196 funded by JCCM and the EU through "Fondo Europeo de Desarrollo Regional" (FEDER); grant 2022-GRIN-34325 funded by UCLM (FEDER). T.H. thanks financial support by Grant-in-Aid for JSPS Research Fellow (JP24KJ1655). M.H. thanks MICIU for the FPI fellowship PRE2021-099064 financed by MICIU/AEI/10.13059/501100011033 and by FSE + . I. H. thanks Hoansha Foundation. The authors thank the Cybermedia Center, The University of Osaka, for use of the Super-computer for Quest to Unsolved Interdisciplinary Datascience (SQUID). The authors acknowledge Ms. R. Miyake at The University of Osaka for HR-MS analysis.

Conflict of Interest

The authors declare no conflict of interest.

Data Availability Statement

The data that support the findings of this study are available in the supplementary material of this article.

Keywords: crystal engineering · flexible porous material · fluorescence · hydrogen-bonded organic framework · pyrene

[1] S. Horike, S. Shimomura, S. Kitagawa, *Nat. Chem.* **2009**, *1*, 695.
[2] S. Seth, S. Jhulki, *Mater. Horiz.* **2021**, *8*, 700.
[3] S. Kitagawa, K. Uemura, *Chem. Soc. Rev.* **2005**, *34*, 109.
[4] V. Guillerm, D. Kim, J. F. Eubank, R. Luebke, X. Liu, K. Adil, M. S. Lah, M. Eddaoudi, *Chem. Soc. Rev.* **2014**, *43*, 6141.
[5] S. Yuan, L. Feng, K. Wang, J. Pang, M. Bosch, C. Lollar, Y. Sun, J. Qin, X. Yang, P. Zhang, Q. Wang, L. Zou, Y. Zhang, L. Zhang, Y. Fang, J. Li, H.-C. Zhou, *Adv. Mate* **2018**, *30*, 1704303.
[6] V. F. Yusuf, N. I. Malek, S. K. Kailasa, *ACS Omega* **2022**, *7*, 44507.
[7] R. Freund, O. Zaremba, G. Arnauts, R. Ameloot, G. Skorupskii, M. Dincă, A. Bavykina, J. Gascon, A. Ejsmont, J. Goscianska, M. Kalmutzki, U. Lächelt, E. Ploetz, C. S. Diercks, S. Wuttke, *Angew. Chem. Int. Ed.* **2021**, *60*, 23975.
[8] K. Geng, T. He, R. Liu, S. Dalapati, K. T. Tan, Z. Li, S. Tao, Y. Gong, Q. Jiang, D. Jiang, *Chem. Rev.* **2020**, *120*, 8814.
[9] Y. Yusran, B. Miao, S. Qiu, Q. Fang, *Acc. Mater. Res.* **2024**, *5*, 1263.
[10] H. Sato, W. Kosaka, R. Matsuda, A. Hori, Y. Hijikata, R. V. Belosludov, S. Sakaki, M. Takata, S. Kitagawa, *Science* **2014**, *343*, 167.
[11] P. Horcajada, R. Gref, T. Baati, P. K. Allan, G. Maurin, P. Couvreur, G. Férey, R. E. Morris, C. Serre, *Chem. Rev.* **2012**, *112*, 1232.
[12] Q. Chen, Z. Chang, W.-C. Song, H. Song, H.-B. Song, T.-L. Hu, X.-H. Bu, *Angew. Chem. Int. Ed.* **2013**, *52*, 11550.
[13] Y. He, S. Xiang, B. Chen, *J. Am. Chem. Soc.* **2011**, *133*, 14570.
[14] R.-B. Lin, Y. He, P. Li, H. Wang, W. Zhou, B. Chen, *Chem. Soc. Rev.* **2019**, *48*, 1362.
[15] I. Hisaki, C. Xin, K. Takahashi, T. Nakamura, *Angew. Chem. Int. Ed.* **2019**, *58*, 11160.
[16] B. Wang, R.-B. Lin, Z. Zhang, S. Xiang, B. Chen, *J. Am. Chem. Soc.* **2020**, *142*, 14399.
[17] X. Song, Y. Wang, C. Wang, D. Wang, G. Zhuang, K. O. Kirlikovali, P. Li, O. K. Farha, *J. Am. Chem. Soc.* **2022**, *144*, 10663.
[18] P. Li, M. R. Ryder, J. F. Stoddart, *Acc. Mater. Res.* **2020**, *1*, 77.
[19] J. Luo, J.-W. Wang, J.-H. Zhang, S. Lai, D.-C. Zhong, *CrystEngComm* **2018**, *20*, 5884.
[20] J. Li, B. Chen, *Chem. Sci.* **2024**, *15*, 9874.
[21] A. Pedrini, D. Marchetti, R. Pinalli, C. Massera, *ChemPlusChem* **2023**, *88*, e202300383.
[22] Q. Zhu, L. Wei, C. Zhao, H. Qu, B. Liu, T. Fellowes, S. Yang, A. Longcake, M. J. Hall, M. R. Probert, Y. Zhao, A. I. Cooper, M. A. Little, *J. Am. Chem. Soc.* **2023**, *145*, 23352.
[23] X. Song, Y. Wang, C. Wang, X. Gao, Y. Zhou, B. Chen, P. Li, *J. Am. Chem. Soc.* **2024**, *146*, 627.
[24] Y. Zhou, C. Chen, R. Krishna, Z. Ji, D. Yuan, M. Wu, *Angew. Chem. Int. Ed.* **2023**, *62*, e202305041.
[25] H. Kubo, S. Konishi, R. Oketani, T. Hayashi, I. Hisaki, *Chem. Eur. J.* **2024**, *30*, e202401645.
[26] H. Wang, B. Li, H. Wu, T.-L. Hu, Z. Yao, W. Zhou, S. Xiang, B. Chen, *J. Am. Chem. Soc.* **2015**, *137*, 9963.
[27] Q. Ji, K. Takahashi, S. Noro, Y. Ishigaki, K. Kokado, T. Nakamura, I. Hisaki, *Cryst. Growth Des.* **2021**, *21*, 4656.
[28] X.-Y. Gao, Y.-L. Li, T.-F. Liu, X.-S. Huang, R. Cao, *CrystEngComm* **2021**, *23*, 4743.
[29] H. Kubo, R. Oketani, I. Hisaki, *Chem. Commun.* **2021**, *57*, 8568.
[30] Z. Xiong, S. Xiang, Y. Lv, B. Chen, Z. Zhang, *Adv. Funct. Mater.* **2024**, *34*, 2403635.
[31] Q. Huang, W. Li, Z. Mao, L. Qu, Y. Li, H. Zhang, T. Yu, Z. Yang, J. Zhao, Y. Zhang, M. P. Aldred, Z. Chi, *Nat. Commun.* **2019**, *10*, 3074.
[32] Q. Huang, W. Li, Z. Mao, H. Zhang, Y. Li, D. Ma, H. Wu, J. Zhao, Z. Yang, Y. Zhang, L. Gong, M. P. Aldred, Z. Chi, *Chem* **2021**, *7*, 1321.
[33] Y. Lv, Z. Xiong, Y. Li, D. Li, J. Liang, Y. Yang, F. Xiang, S. Xiang, Y. S. Zhao, Z. Zhang, J. Phys, *Chem. Lett.* **2022**, *13*, 130.
[34] Y. Lv, J. Liang, Z. Xiong, X. Yang, Y. Li, H. Zhang, S. Xiang, B. Chen, Z. Zhang, *Adv. Mater.* **2024**, *36*, 2309130.
[35] Q. Huang, X. Chen, W. Li, Z. Yang, Y. Zhang, J. Zhao, Z. Chi, *Chem* **2023**, *9*, 1241.
[36] Y. Shi, Y. Ding, W. Tao, P. Wei, *ACS Appl. Mater. Interfaces* **2022**, *14*, 36071.
[37] Q. Huang, W. Li, Z. Yang, J. Zhao, Y. Li, Z. Mao, Z. Yang, S. Liu, Y. Zhang, Z. Chi, *CCS Chemistry* **2021**, *4*, 1643.
[38] M. Liang, S. Hu, N. Zhou, Z. Liu, Q. Chen, X. Chen, X. Liu, C.-P. Li, J. Hao, P. Xue, *Small* **2023**, *19*, 2304340.
[39] S. Wang, J. Liu, S. Feng, J. Wu, Z. Yuan, B. Chen, Q. Ling, Z. Lin, *Angew. Chem. Int. Ed.* **2024**, *63*, e202400742.
[40] T. Hinoue, M. Miyata, I. Hisaki, N. Tohnai, *Angew. Chem. Int. Ed.* **2012**, *51*, 155.
[41] D. Kraskouskaya, M. Bancerz, H. S. Soor, J. E. Gardiner, P. T. Gunning, *J. Am. Chem. Soc.* **2014**, *136*, 1234.
[42] K. Ayyavoo, P. Velusamy, *New J. Chem.* **2021**, *45*, 10997.
[43] D. Ning, Q. Liu, Q. Wang, X.-M. Du, Y. Li, W.-J. Ruan, *Dalton Trans.* **2019**, *48*, 5705.
[44] S. Hu, L. Hu, X. Zhu, Y. Wang, M. Liu, *Angew. Chem. Int. Ed.* **2021**, *60*, 19451.
[45] T. M. Figueira-Duarte, K. Müllen, *Chem. Rev.* **2011**, *111*, 7260.
[46] F. P. Kinik, A. Ortega-Guerrero, D. Ongari, C. P. Ireland, B. Smit, *Chem. Soc. Rev.* **2021**, *50*, 3143.
[47] P. Shen, H. Xu, T. Zhao, W. Zhang, G. Bai, T. Alshahrani, B. Chen, J. Gao, S. Xu, *Microporous Mesoporous Mater.* **2025**, *381*, 113348.
[48] T. Hashimoto, R. Oketani, A. Inoue, K. Okubo, K. Oka, N. Tohnai, K. Kamiya, S. Nakanishi, I. Hisaki, *Chem. Commun.* **2023**, *59*, 7224.
[49] L. He, Y. Li, L. Li, Z. Wang, Y. Chen, F. Yuan, G. Lan, C. Chen, S. Xiang, B. Chen, Z. Zhang, *Angew. Chem. Int. Ed.* **2025**, *64*, e202418917.
[50] A. Wrona-Piotrowicz, A. Makal, J. Zakrzewski, *J. Org. Chem.* **2020**, *85*, 11134.
[51] X. Feng, J.-Y. Hu, F. Iwanaga, N. Seto, C. Redshaw, M. R. J. Elsegood, T. Yamato, *Org. Lett.* **2013**, *15*, 1318.
[52] K. Nakano, K. Sada, Y. Kurozumi, M. Miyata, *Chem. Eur. J.* **2001**, *7*, 209.
[53] S. Tsuzuki, K. Honda, T. Uchimaru, M. Mikami, K. Tanabe, *J. Am. Chem. Soc.* **2000**, *122*, 3746.
[54] S. Tsuzuki, K. Honda, T. Uchimaru, M. Mikami, K. Tanabe, *J. Am. Chem. Soc.* **2002**, *124*, 104.
[55] S. Reiter, M. K. Roos, R. de Vivie-Riedle, *ChemPhotoChem* **2019**, *3*, 881.
[56] T. Costa, J. Seixas de Melo, H. D. Burrows, *J. Phys. Chem. B* **2009**, *113*, 618.
[57] V. Vangani, J. Drage, J. Mehta, A. K. Mathew, J. Duhamel, *J. Phys. Chem. B* **2001**, *105*, 4827.
[58] J. Kusz, C. Boissiere, Y. Bretonnière, C. Sanchez, S. Parola, *Nanoscale* **2024**, *16*, 18918.
[59] T. Fujii, E. Shimizu, *Chem. Phys. Lett.* **1987**, *137*, 448.
[60] G. K. Bains, S. H. Kim, E. J. Sorin, V. Narayanaswami, *Biochemistry* **2012**, *51*, 6207.
[61] R. D. Pensack, R. J. Ashmore, A. L. Paoletta, G. D. Scholes, *J. Phys. Chem. C* **2018**, *122*, 21004.
[62] L. R. Williams, E. B. Gamble, K. A. Nelson, S. De Silvestri, A. M. Weiner, E. P. Ippen, *Chem. Phys. Lett.* **1987**, *139*, 244.
[63] J. Hoche, H.-C. Schmitt, A. Humeniuk, I. Fischer, R. Mitrić, M. I. S. Röhr, *Phys. Chem. Chem. Phys.* **2017**, *19*, 25002.
[64] T. Hashimoto, M. de la Hoz Tomás, R. Oketani, B. Cohen, M. Naruoka, N. Tohnai, A. Douhal, I. Hisaki, *Angew. Chem. Int. Ed.* **2025**, *64*, e202419992.
[65] I. Hisaki, N. Ikenaka, E. Gomez, B. Cohen, N. Tohnai, A. Douhal, *Chem. Eur. J.* **2017**, *23*, 11611.
[66] I. Hisaki, Y. Suzuki, E. Gomez, B. Cohen, N. Tohnai, A. Douhal, *Angew. Chem. Int. Ed.* **2018**, *57*, 12650.
[67] C. F. Macrae, I. Sovago, S. J. Cottrell, P. T. A. Galek, P. McCabe, E. Pidcock, M. Platings, G. P. Shields, J. S. Stevens, M. Towler, P. A. Wood, *J. Appl. Crystallogr.* **2020**, *53*, 226.
[68] Gaussian 16, Revision C.01, M. J. Frisch, G. W. Trucks, H. B. Schlegel, G. E. Scuseria, M. A. Robb, J. R. Cheeseman, G. Scalmani, V. Barone, G. A. Petersson, H. Nakatsuji, X. Li, M. Caricato, A. Marenich, J. Bloino, B. G. Janesko, R. Gomperts, B. Mennucci, H. P. Hratchian, J. V. Ortiz, A. F. Izmaylov, J. L. Sonnenberg, D. Williams-Young, F. Ding, F. Lipparini, F. Egidi, J. Goings, B. Peng, A. Petrone, T. Henderson, D. Ranasinghe, V. G. Zakrzewski, J. Gao, N. Rega, G. Zheng, W. Liang, M. Hada, M. Ehara, K. Toyota, R. Fukuda, J. Hasegawa, M. Ishida, T. Nakajima, Y. Honda, O. Kitao, H. Nakai, T. Vreven, K. Throssell, J. A. Montgomery, Jr., J. E.

Peralta, F. Ogliaro, M. Bearpark, J. J. Heyd, E. Brothers, K. N. Kudin, V. N. Staroverov, T. Keith, R. Kobayashi, J. Normand, K. Raghavachari, A. Rendell, J. C. Burant, S. S. Iyengar, J. Tomasi, M. Cossi, J. M. Millam, M. Klene, C. Adamo, R. Cammi, J. W. Ochterski, R. L. Martin, K. Morokuma, O. Farkas, J. B. Foresman, D. J. Fox, Gaussian, Inc., Wallingford CT, **2019**.
[69] Rigaku Oxford Diffraction **2015**, *Software CrysAlisPro 1.171.38.41o*. Rigaku Corporation, Tokyo, Japan.
[70] G. M. Sheldrick, *Acta Crystallogr. A Found. Adv.* **2015**, *71*, 3.
[71] O. V. Dolomanov, L. J. Bourhis, R. J. Gildea, J. A. K. Howard, H. Puschmann, *J. Appl. Crystallogr.* **2009**, *42*, 339.
[72] L. J. Bourhis, O. V. Dolomanov, R. J. Gildea, J. A. K. Howard, H. Puschmann, *Acta Crystallogr. A Found. Adv.* **2015**, *71*, 59.
[73] G. M. Sheldrick, *Acta Crystallogr. C Struct. Chem.* **2015**, *71*, 3.
[74] P. van der Sluis, A. L. Spek, *Acta Crystallogr. A Found. Adv.* **1990**, *46*, 194.
[75] A. L. Spek, *Acta Crystallogr. D Biol. Crystallogr.* **2009**, *65*, 148.
[76] E. Gomez, M. Gutiérrez, B. Cohen, I. Hisaki, A. Douhal, *J. Mater. Chem. C* **2018**, *6*, 6929.
[77] A. G. Crawford, A. D. Dwyer, Z. Liu, A. Steffen, A. Beeby, L.-O. Pålsson, D. J. Tozer, T. B. Marder, *J. Am. Chem. Soc.* **2011**, *133*, 13349.

Manuscript received: June 23, 2025
Revised manuscript received: July 7, 2025
Version of record online: July 25, 2025